Carbohydrate Polymers 120 (2015) 38–45

Contents lists available at ScienceDirect

Carbohydrate Polymers

journal homepage: www.elsevier.com/locate/carbpol

Microfluidic fabrication of shape-tunable alginate microgels: Effect of size and impact velocity

Yuandu Hu[a], Glareh Azadi[a], Arezoo M. Ardekani[a,b,*]

[a] Department of Aerospace and Mechanical Engineering, University of Notre Dame, Notre Dame, IN 46556, United States
[b] School of Mechanical Engineering, Purdue University, 585 Purdue Mall, West Lafayette, IN 47907, United States

ARTICLE INFO

Article history:
Received 25 June 2014
Received in revised form
20 November 2014
Accepted 21 November 2014
Available online 9 December 2014

Keywords:
Microfluidics
Non-spherical alginate microgels
Microgel superstructures

ABSTRACT

We report on a capillary-based microfluidic platform for the fabrication of non-spherical sodium alginate microgels. The sodium alginate droplets were crosslinked off-chip in a mixture of barium acetate and glycerol solution. Novel morphologies such as tear drop, lamp-like, mushroom-like, double-dimpled and bowl-like microgels were fabricated by controlling the size, impact velocity (at the crosslinking solution/oil interface), and concentration of sodium alginate solution. We monitored the microscale deformation process *in situ* at the interface and proposeed a deformation mechanism resulting in unique morphologies. Additionally, we constructed microgel superstructures by assembling the non-spherical alginate microgels to spherical poly(*N*-isopropylacrylamide) (pNIPAAm) microgels *via* electrostatic interaction.

1. Introduction

Sodium alginate is a natural polysaccharide based copolymer composed of β-D-mannuronic acid (***M***) and α-L-guluronic acid (***G***) on the linear chain (Lee & Mooney, 2012). The binding of G blocks to divalent ions such as Ca^{2+} and Cu^{2+}(crosslinking) results in the formation of three dimensional structures, known as hydrogels (Asthana, Kim, Perumal, Kim, & Kim, 2009; Bajpai & Sharma, 2004; Bonino et al., 2011; Gazori et al., 2009; Liakos et al., 2013). Owing to biocompatibility and mild crosslinking conditions, alginate-based microgels have gained increasing attention in the field of drug release (Lin, Yang, Hsu, & Hsieh, 2013), protein, antibodies and cell encapsulation (Qiu, Chen, Yan, & Wu, 2007; Tan & Takeuchi, 2007), and encoding (Ji et al., 2011). Among numerous fabrication techniques including extrusion–dripping (Chan, Lee, Ravindra, & Poncelet, 2009), centrifuge-based (Maeda, Onoe, Takinoue, & Takeuchi, 2012), cast-strategy (Wang, Cui, Li, & van Hest, 2012) and soft-lithography (Qiu, Chen, Yan, & Wu, 2007), microfluidic techniques are widely employed, allowing for the fabrication of size tunable monodispersed microgels with customized morphologies and chemical properties (Zhao et al., 2013; Nisisako, Torii, Takahashi, & Takizawa, 2006; Lee et al., 2012; Hu et al., 2013; Shang et al., 2013; Kanai, Lee, Shum, Shah, & Weitz, 2010; Kang et al., 2014; Liu, Deng, Li, & Zhu, 2012). Microfluidic fabrication of alginate microgels employs a water/oil emulsion mechanism, with two immiscible solutions: aqueous solution of sodium alginate as the dispersed phase, and oil/organic solution as the continuous phase. The gelation or crosslinking step is followed by the addition of cationic divalent ions through an internal or external procedure which can be achieved both on-chip and off-chip. In the external on-chip gelation process, the crosslinking agent is mixed with the continuous phase, whereas in the internal gelation process, nanoparticles of the crosslinking agent are embedded within the aqueous phase and ionized by a reduction in pH (Marquis, Davy, Fang, & Renard, 2014; Tan & Takeuchi, 2007).

Microparticle morphology is an influential factor in many applications such as, intracellular delivery of particles (Muro et al., 2008), stability of particles in emulsions (Madivala, Vandebril, Fransaer, & Vermant, 2009), colloidal interactions at liquid–liquid interface or within the solvent (Loudet, Alsayed, Zhang, & Yodh, 2005; Mondiot, Chandran, Mondain-Monval, & Loudet, 2009), and Brownian motion (Han et al., 2006), and 3D tissue formation (Du, Lo, Ali, & Khademhosseini, 2008).

Apart from the common spherical morphology, non-spherical microgels are highly desirable due to the anisotropic responses to the external forces, and the large surface area. In addition, these microgels can be used as building blocks in modeling of complex macromolecules (Lu, Yin, & Xia, 2001; Yoo & Mitragotri, 2010). Several groups have demonstrated the microfluidic fabrication of non-spherical microgels using UV polymerization (Dendukuri, Pregibon, Collins, Hatton, & Doyle, 2006; Xu et al., 2005).

* Corresponding author at: School of Mechanical Engineering, Purdue University, 585 Purdue Mall, West Lafayette, Indiana 47907, United States. Tel.: +1 765 4960002.
E-mail address: ardekani@purdue.edu (A.M. Ardekani).

http://dx.doi.org/10.1016/j.carbpol.2014.11.053
0144-8617/

However, crosslinking with UV is limited to the light sensitive polymers and is not suitable for biological applications. Zhao and coworkers reported fabrication of plug-like, and disk-like alginate microgels using an on-chip crosslinking process (Liu, Ding, Liu, Chen, & Zhao, 2006). Other morphologies such as tailed-shape, mushroom-like and torus microgels have been reported using off-chip crosslinking of alginate droplets. In this process, spherical droplets are collected in a crosslinking solution and deformed as they pass through the interface of the crosslinking solution (Capretto, Mazzitelli, Luca, & Nastruzzi, 2010; Hu et al., 2012; Lin, Yang, Hsu, & Hsieh, 2013; Mele et al., 2013). In light of an increasing demand for the fabrication of microgels with a wide range of morphologies, in this study we report on the microfluidic fabrication of non-spherical alginate microgels based on an off-chip crosslinking process. The present technique allows us to simply tune the morphology of the microgels by changing the impact velocity of the droplets, which is achieved by changing the distance between the tip of the collecting tube and the interface of crosslinking solution, called hereafter collecting height. A significant volume of reported studies in the literature has focused on the final morphology of microgels (end result). In the present work, for the first time we monitored the microscale deformation of droplets in real time, at the air–solution interface (*in situ*) with the use of a high speed camera. Furthermore, we determined the driving mechanisms governing morphological changes at the interface. Factors considered were droplet size, collecting height, and the concentration of the dispersed phase (sodium alginate). Our results provide fundamental insights on the microscale deformation of droplets, and can be extended to the fabrication of microgels with customized morphology and chemical properties toward specific biological applications. Furthermore, uniform spherical pNIPAAm microgels were fabricated using a capillary-based microfluidic platform. The pNIPAAm microgels were assembled with double-dimpled alginate microgels by the electrostatic interaction between particles. We note that the pNIPAAm microgel can interact with different numbers of double-dimpled alginate microgels and form microgel superstructures. Superstructures possess different conformations and can be used to understand the structure of macromolecules, and for the construction of complex lock–key particles and self-propelled particles (Hong, Cacciuto, Luijten, & Granick, 2006; Wang et al., 2014; Yi, Pine, & Sacanna, 2013).

2. Experimental

2.1. Materials

Sodium alginate at 1.5 wt% and 2 wt% concentration (Sigma–Aldrich; St. Louis, MO; W201502) with 396 kDa MW and M/G = 1.49 (Dalmoro, Angela, Lamberti, Grassi, & Amore, 2012) was used as the dispersed phase. The continuous phase was composed of 5 wt% non-ionic surfactant Cetyl PEG/PPG-10/1 Dimethicone (Abil EM90) (Evonik industries; Mapleton, IL) in Hexadecane (Sigma–Aldrich; H6703, 99% purity). A mixture of 10 wt% barium acetate (Sigma–Aldrich; 243671, 99% purity) and 50 wt% glycerol (Sigma–Aldrich; G5516, 99% purity) was used as the crosslinking solution. All compounds were used as received. Aqueous solutions were prepared in ultrapure deionized water (Barnestead Nanopure II; Thermofisher Scientific, Waltham, MA). Capillary based microfluidic devices were constructed from round (580 μm ID) and square (1 mm ID) glass capillaries (Vitrocom; Mountain Lakes, NJ).

2.2. Microfluidic fabrication of monodispersed droplets

Two tapered round glass capillaries (580 μm ID) with different orifice size (387 μm, 87 μm) were coaxially inserted into a square glass capillary (1 mm ID). The separation between the orifices was 50 μm. Droplets were fabricated in a co-flow set up where the two phases flow in the same direction. The aqueous phase flows inside the round capillaries, while the oil phase flows between the round and square capillaries. Detailed description of the microfluidic setup can be found in a previous publication (Shah et al., 2008).

The aqueous and oil phases were injected in the microfluidic device using two syringe pumps (Harvard Apparatus, NE 1000, Holliston, MA). The droplet diameter was tuned by changing the flow rate of the continuous phase and orifice diameter of the injecting tube. Fig. 1 shows a schematic of the microfluidic device, collecting methods, and various morphologies obtained by manipulating the impact velocity (collecting height), droplet diameter, and sodium alginate concentration.

2.3. Spherical microgels

Monodispered spherical droplets with 190 μm diameter were fabricated in a microfluidic device with the orifices of round capillaries at 260 μm and 70 μm. The flow rates of continuous and dispersed phases were constant at 2300 μl/h and 30 μl/h, respectively. Alginate droplets were continuously delivered to the crosslinking solution by a soft silicone tube (0.015 inch ID, Thermofisher Scientific). To avoid droplet deformation, the tube was mounted parallel and in close proximity of the interface of the collecting solution (Fig. 1a).

2.4. Non-spherical microgels

The fabrication of non-spherical microgels was accomplished by increasing the collecting height *h* from the tip of the tube to the air–solution interface shown in Fig. 1b and consequently increasing the impact velocity. Droplets of 190 μm diameter were generated and three collecting heights of 0 mm (2.1 mm/s), 5 mm (2.8 mm/s) and 10 mm (3.5 mm/s) were examined. To avoid aggregation of the droplets at the tip of the tube, the tube was positioned in contact with the inner wall of the container, above the air–solution interface. As shown in Fig. 1b, the solution interface is a double layer, composed of a thin oil layer and the aqueous crosslinking layer. Upon contact with the solution, the droplets (density 0.998 g/cm^3 for 1.5% sodium alginate), pass through the oil layer (density 0.798 g/cm^3), and float at the aqueous/oil interface, due to a smaller density compared to the crosslinking solution (density 1.12 g/cm^3). The floating time is determined by the droplet diameter and impact velocity. The crosslinking of the droplets initiates at the lower end which is the point of contact with Ba^{2+}. The diffusion of Ba^{2+} and simultaneous gelation result in an increase in the density and a gradual settling within the solution. The viscosity of the crosslinking solution was measured as 0.01 Pa s.

3. Results and discussion

Alginate droplets are continuously formed in the flow focusing section of the device with a dripping mode achieved by Rayleigh–Plateau instability (Fig. 2a). Fig. 2b shows the monodispersed alginate droplets prior to crosslinking. Droplets with different diameters can be fabricated by changing the flow rate of the oil phase (Fig. 2c). Compared to the Newtonian oil phase (viscosity 3.8 mPa s), sodium alginate solutions display a typical shear thinning behavior (Hu et al., 2012) (Fig. 2d). This is evident by a reduction in viscosity from 60 mPa s at shear rate of 0.1 s^{-1} to 30 mPa s at shear rate of 10 s^{-1}. The higher viscosity of alginate solutions, compared to that of oil (one order of magnitude) reduces the focusing capability of the oil phase (Martinez et al., 2012; Nie et al., 2008). This in turn enhances the ability to fabricate droplets with a small variation in diameter (60 μm range in Fig. 2c).

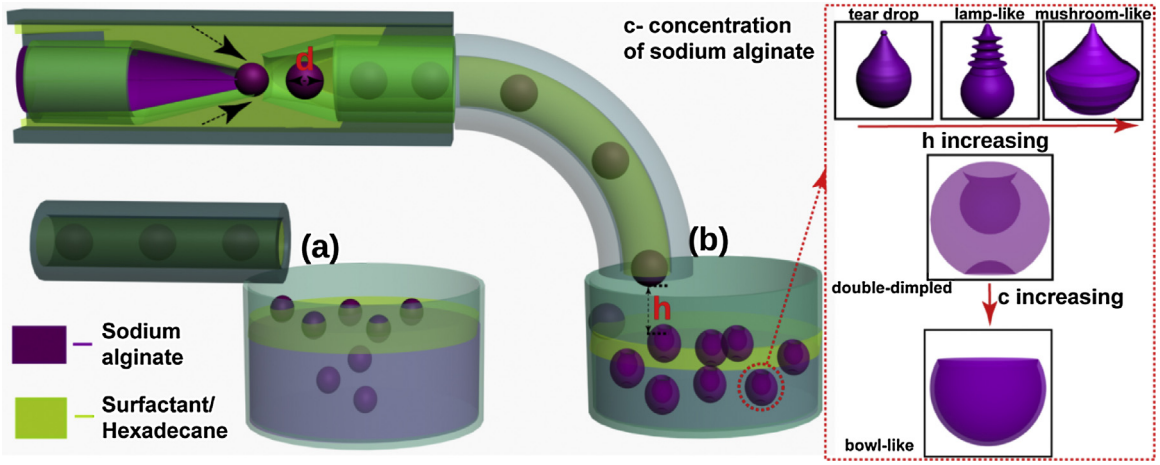

Fig. 1. Schematic of a co-flow capillary-based microfluidic device. Off-chip crosslinking was achieved by mounting the collecting tube (a) parallel and (b) normal to the interface of the collecting solution to fabricate spherical and non-spherical droplets, respectively. Tear drop, lamp-like and mushroom-like microgels were fabricated from droplets collected at different heights (h) with a constant diameter (190 μm). Double-dimpled (1.5% sodium alginate) and bowl-shaped (2% sodium alginate) microgels were resulted from increasing the initial droplet diameter to 250 μm while keeping (h) constant at 10 mm.

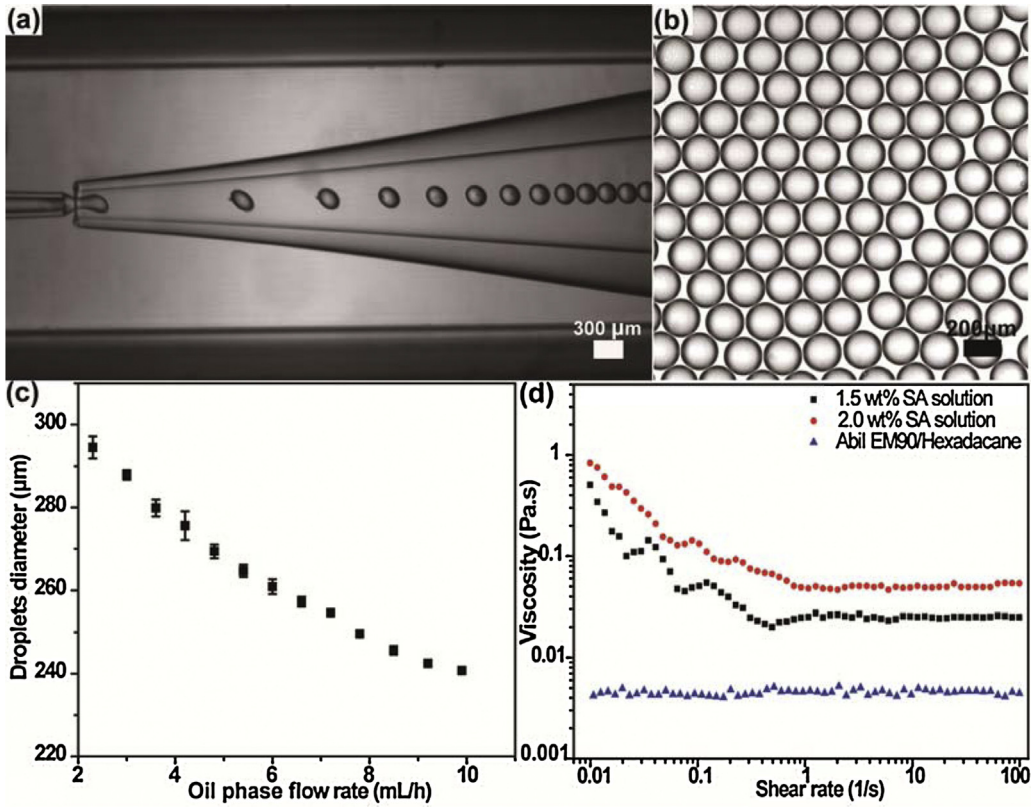

Fig. 2. Optical microscope image of (a) the droplet formation in a capillary microfluidic device. (b) monodispersed droplets. (c) Variation of droplet diameter with the flow rate of oil phase. (d) Viscosity of oil and aqueous phases as a function of shear rate.

Fig. 3a shows monodispersed spherical droplets of 190 μm in the crosslinking solution at time zero. After about 20 min, the diameter is reduced to 140 μm (Fig. 3b). The 26% reduction in diameter is attributed to the release of water from the droplets into the crosslinking solution (Hirama et al., 2013; Marquis, Davy, Fang, & Renard, 2014) due to the difference in the osmotic pressure. The osmotic pressure for the crosslinking solution, and 1.5 wt% and 2 wt% alginate solutions are reported as 9.6 MPa, 63 kPa and 75 kPa, respectively (Wang & Bloomfield, 1990). The difference in osmotic pressure results in the outward diffusion of water from the droplet and inward diffusion of Ba^{2+} from the crosslinking solution and simultaneous crosslinking of the droplets. The droplet undergoes further reduction in size with time (Fig. 3c). It is important to note that all the droplets do not crosslink at the same time. This is mainly due to the presence of an oil layer, with a decreasing thickness away from the tip of the collecting tube (progressing yellow circles in Fig. 3). Therefore, the rate of crosslinking process is slower for the droplets located in the vicinity of a thicker oil layer, where the diffusion of Ba^{2+} is limited. In addition, owing to different refractive indices between alginate hydrogel (1.37 at 20 °C) and water (1.33 at 20 °C), the optical properties change as a function of time due to continuous crosslinking (Daimon & Masumura, 2007; Esteban, Marvá, & Martínez-Antón, 2009). This is evident by a change in contrast comparing the droplets (before crosslinking) and microgels

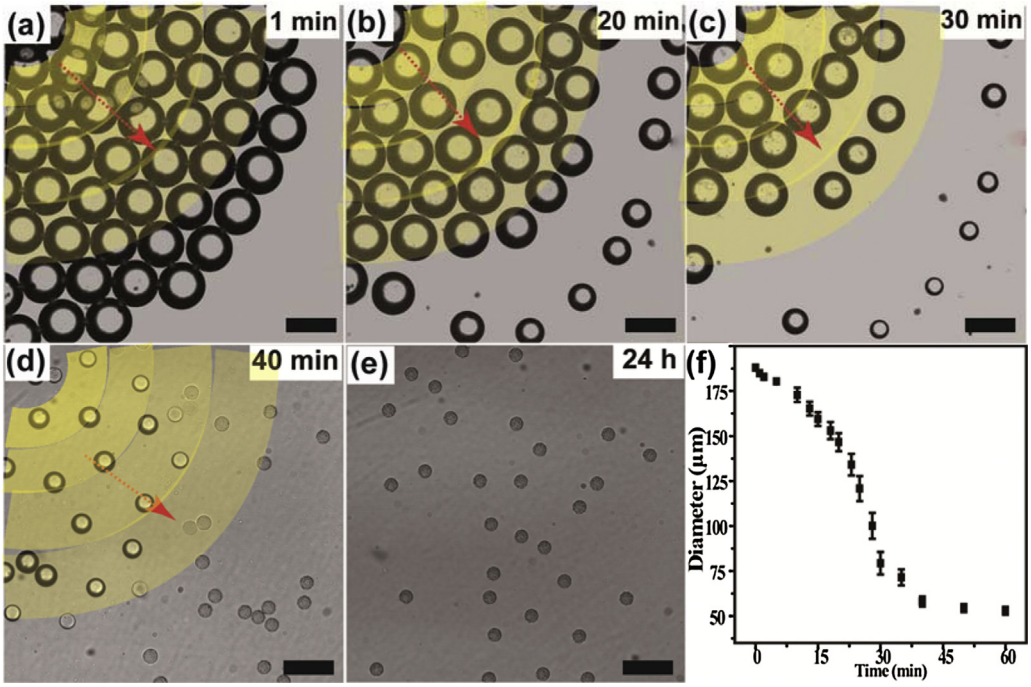

Fig. 3. Evolution of spherical droplets to microgels as a function of incubation time inside the crosslinking solution: (a) 1 min, (b) 20 min, (c) 30 min, (d) 40 min, and (e) 24 h. Scale bars show 200 μm. Progressing yellow circles schematically shows that the thickness of the oil phase reduces away from the tip of the collecting tube (in the direction of the red arrow). (f) Variation of droplet diameter as a function of time. (For interpretation of the references to color in this figure legend, the reader is referred to the web version of this article.)

(after crosslinking). Our results show that droplets located at 1.6 mm from the collecting tube are fully crosslinked in 40 min (Fig. 3d). After 24 h, all of the droplets are fully crosslinked and settled to the bottom of the container (Fig. 3e). Continuous reduction of diameter as a function of crosslinking time is shown in Fig. 3f.

Non-spherical microgels were fabricated by increasing the collecting height/impact velocity. We studied the effect of the collecting height on the final morphology of the microgels at collecting heights 0, 5, and 10 mm (2.1 mm/s, 2.8 mm/s and 3.5 mm/s) with 190 μm droplets. Fig. 4a shows the spherical morphology of droplets before impact at the air–solution interface. Droplet velocities were calculated using a series of images captured by a high speed camera at 60 f/s (SA4 Fastcam, Photron). Fig. 4b–d shows different morphologies of microgels collected at 0 mm, 5 mm and 10 mm. The resulting microgels demonstrated unique tailed morphologies as: tear drop (Fig. 4b), lamp-like (Fig. 4c, with rims around the neck Fig. 4e) and mushroom-like (Fig. 4d). The velocity of 190 μm droplets increases with the increase in the collecting height as shown in Fig. 4f.

In order to study the effect of the droplet diameter on the final morphology of microgels, we increased the diameter of droplets to 250 μm (for better visualization at the interface) while keeping the collecting distance and alginate concentration constant at 10 mm and 1.5 wt%, respectively. Fig. 5a shows the formation of double-dimpled microgels. To observe the deformation process at the solution interface, images of the droplet at the interface were captured at 60 f/s by a high speed camera (SA4 Fastcam, Photron) at 12× magnification. For these *in situ* studies the droplet impact velocity was 5 mm/s. We hypothesize that the deformation of microdroplets, affected by their impact velocities, occurs at the interface of the oil and the crosslinking solution. This means that the final microgel morphology is determined at the solution interface. Once the droplet passes through the interface, the density of the droplet increases due to the crosslinking process and the diffusion of Ba^{2+} within the droplets. Fig. 5b shows the initial stages of deformation at the point of contact with the crosslinking solution. The difference in the osmotic pressure between the droplets and crosslinking solution results in the outward diffusion of water molecules and a reduction in droplet diameter over time (Fig. 5c–e). After 45 min, a significant volume of the spherical droplet is submerged in the crosslinking solution (Fig. 5d). Rapid deformation follows at 46 min, creating a dimpled droplet (Fig. 5e). A possible mechanism for crosslinking at the interface is demonstrated in Fig. 5h. Initial crosslinking at the bottom of the droplet create inhomogeneous local contractions due to the polymer chain shrinkage. This in turn pulls the polymer chain at the bottom of the droplet toward the center and forms a slightly dimpled spot. After the completion of crosslinking at the surface, the diffusion rate of Ba^{2+} to the inner section of the drop is reduced. Finally, the top portion of the droplet, which is the last section undergoing crosslinking process, is pulled into the center of the droplet (Fig. 5e–f). Further crosslinking results in the development of a cavity, in about 1 min, at the top portion of the droplet (Fig. 5f). The final morphology demonstrated two distinct parts: an apparent big cavity at the top and a small dimple at the bottom (Fig. 5g and inset). It is important to note that, similar double-dimpled morphology was observed when the initial droplet diameter was larger than 250 μm, (Fig. 5i and inset). The observed 50% reduction in diameter agrees well with the reported value in the literature (Lee, Ravindra, & Chan, 2013).

In addition to the effect of the impact velocity and diameter, we explored the morphological changes as a function of alginate concentration. Fig. 6a shows thin-rim bowl-like microgels obtained from 2 wt% sodium alginate droplets with 250 μm diameter and 5 mm/s impact velocity. Fig. 6b–g shows the evolution of the droplet at the interface. Compared to 1.5 wt% alginate, the deformation occurred at a faster rate, and the detention time at the interface was reduced by 82% (45 min with 1.5 wt% and 8 min with 2 wt%). This can be attributed to an increase in droplet density (1.002 g/cm^3). The temporal evolution of droplet shows buckling from the weakest point of the droplet (top portion) upon crosslinking (Fig. 6b–g) (Datta et al., 2012). This process continues with time and completes in 2 min creating a bowl-like microgel (Fig. 6f–g). The thickness of

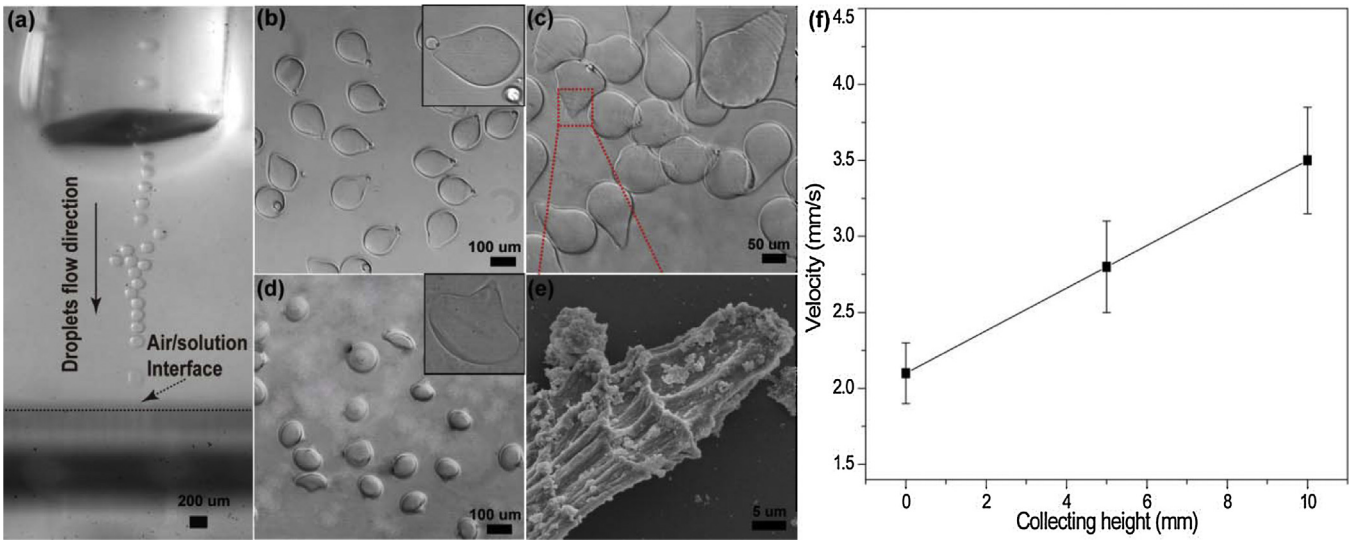

Fig. 4. (a) Spherical droplets (190 μm) before contacting with the crosslinking solution (b–d). Optical microscope images of tear drop, lamp-like and mushroom-like microgels collected at 0 mm, 5 mm and 10 mm, respectively. (e) Scanning electron microscopy (SEM) image of microgels showing the presence of rims around the neck of microgels in (c). (f) Plot of droplets velocity at different collecting heights.

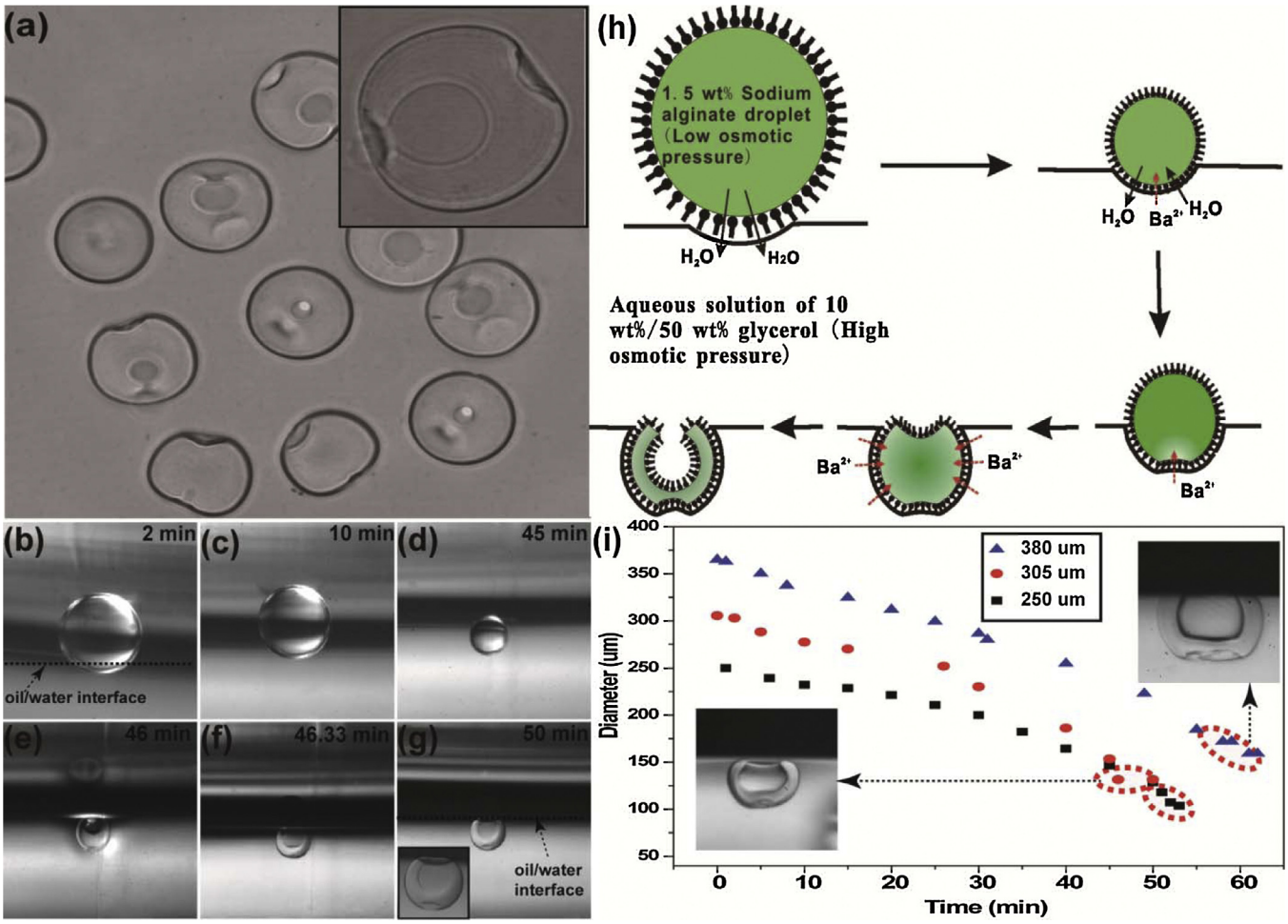

Fig. 5. (a) Optical microscopy image of microgels formed from 250 μm droplets with two dimpled parts in the opposite poles. (b–g) Temporal evolution of the formation of double dimpled microgels at the interface. (h) Schematic of the deformation mechanism at the interface. (i) Variation of droplet diameter as a function of time for droplets with different initial diameters 250 μm, 305 μm, and 380 μm. Red dotted circles mark the starting point of the deformation. (For interpretation of the references to color in this figure legend, the reader is referred to the web version of this article.)

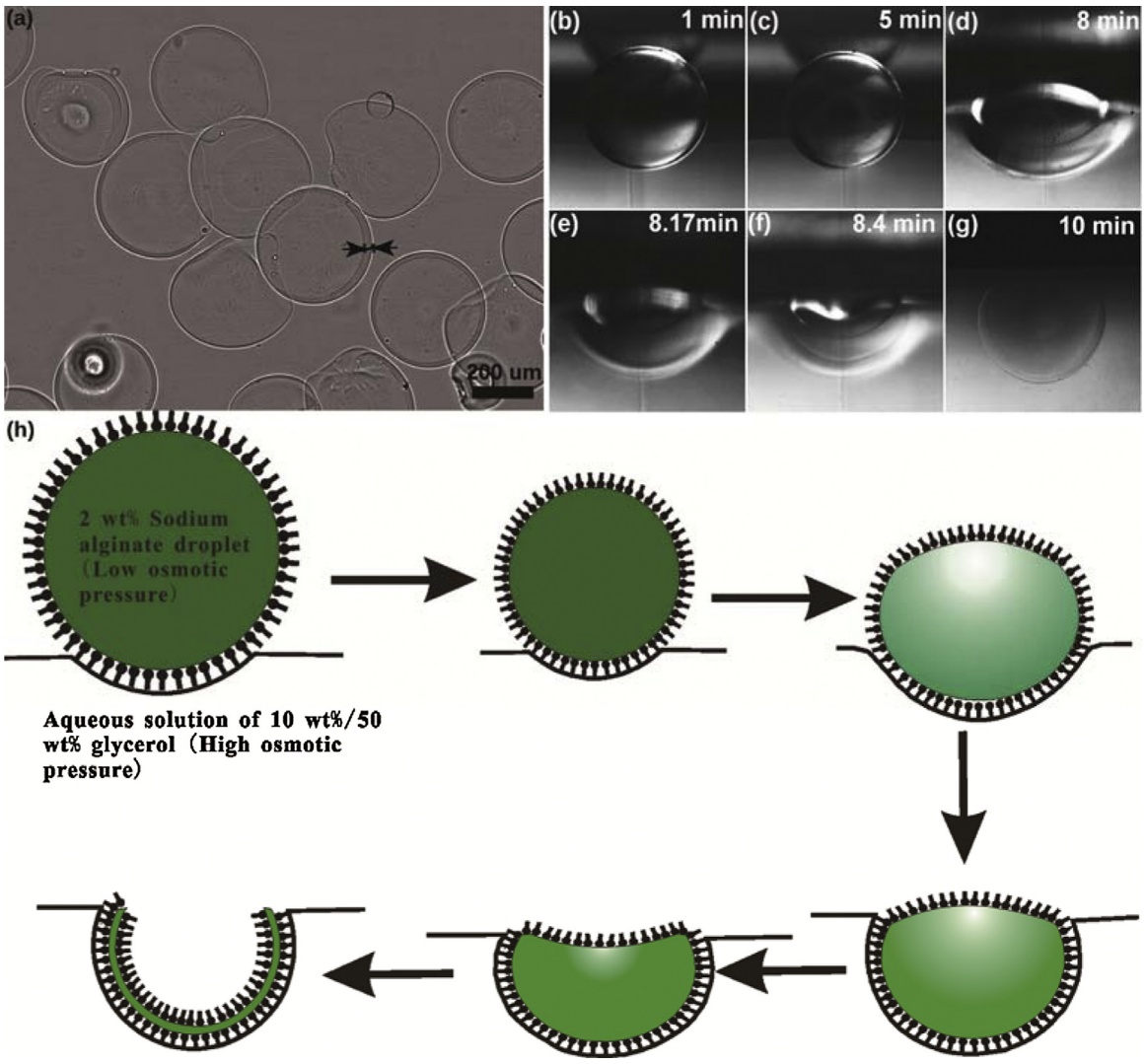

Fig. 6. (a) Optical microscope image of bowl-like microgels formed with increasing sodium alginate concentration to 2 wt% for a droplet with 250 μm diameter. (b–g) The formation of bowl-like microgel at the interface. (h) Schematic of the deformation process at the interface.

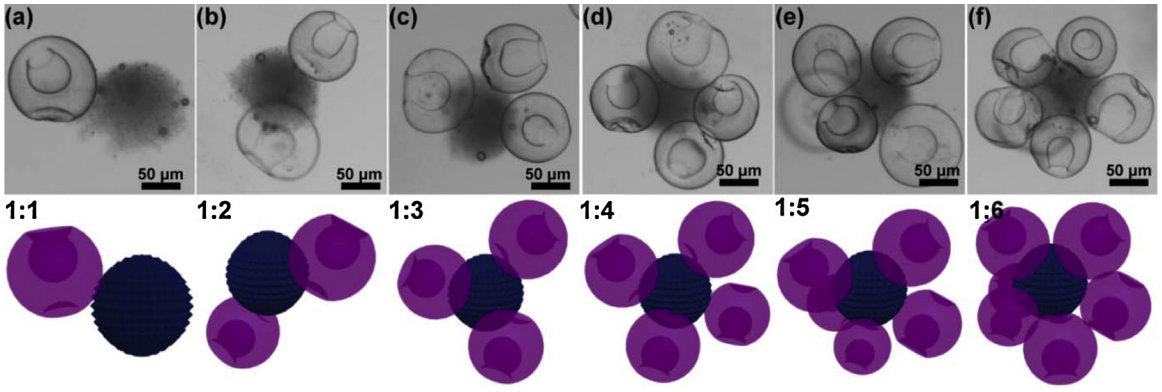

Fig. 7. The superstructure gel particles formed from double-dimpled alginate microgels and pNIPAAm microgels. PNIPAAm microgels can attach to different number of double-dimpled microgels (the value varied from 1 to 6).

the bowl rim can be as small as 30 μm. Fig. 6h shows the proposed mechanism for the deformation at the interface.

Microgel particles can be also used as building blocks in macromolecule assemblies to study their complex structures (Erb, Son, Samanta, Rotello, & Yellen, 2009; Tian et al., 2011; Yan, Bloom, Bae, Luijten, & Granick, 2012). Fig. 7 shows complex structures obtained by the interaction of pNIPAAm microgel and double-dimpled alginate microgels. Clearly, the pNIPAAm microgel can interact with one or more (maximum of 6) alginate microgels to form a microgel superstructure. The driving force for this assembly is the electrostatic interaction between the positively charged pNIPAAm microgel and negatively charged alginate microgels (Fiddes, Young,

Kumacheva, & Wheeler, 2007; Still, Chen, Alsayed, Aptowicz, & Yodh, 2013). More importantly, the alginate microgels are preferentially assembled in non-dimpled area due to the relative weak electrostatic interaction in the dimpled area compared to the non-dimpled area. These microgel superstructures can be potentially extended to smaller scale particles and construction of stereospecific assembly materials (Hong, Cacciuto, Luijten, & Granick, 2006; Wang et al., 2014; Yi, Pine, & Sacanna, 2013; Zamanian et al., 2010).

4. Conclusions

We employed a simple platform for the fabrication of monodispered shape-tunable alginate microgels using a capillary-based microfluidic device combined with an off-chip crosslinking process. Our results show that in an off-chip crosslinking based on collecting the droplets in a crosslinking solution, the final morphology is determined at the solution interface. This morphology is influenced by the impact velocity, droplet size and concentration of alginate solution. We demonstrated the formation of novel morphologies such as tear drop, lamp-like, and mushroom-like microgels obtained from 1.5 wt% sodium alginate droplets with 190 μm diameter and impact velocities of 2.1 mm/s, 2.8 mm/s and 3.5 mm/s, respectively. Increasing the droplet size to 250 μm with a 5 mm/s impact velocity resulted in the formation of double-dimpled microgels. Finally, bowl-shaped droplets were obtained by increasing the concentration of sodium alginate from 1.5 wt% to 2 wt%, with 250 μm droplets and 5 mm/s velocity. In addition, we showed that above a certain diameter (250 μm), double-dimpled morphology is achieved with 1.5 wt% sodium alginate droplets. Based on these observations, we proposed a mechanism for the microscale crosslinking of droplets at the interface, highlighting the effect of osmotic pressure, diffusion rate of crosslinking ions, and the order at which different sections of the droplet undergo crosslinking. Due to a higher density compared to the oil layer and a lower density compared to that of the crosslinking solution, the alginate droplets pass through the oil phase and float at the interface of oil and crosslinking solution. Therefore, the bottom portion of the droplet is the first point of contact for the diffusion of Ba^{2+} inside the droplets. Simultaneously, water molecules diffuse out of the droplets due to differences in osmotic pressure. Upon the completion of the crosslinking of the outer layer (surface), the diffusion rate of Ba^{2+} is reduced, allowing for the center of the droplet to be susceptible to deformation. Depending on the concentration of the alginate solution, the droplets exhibit different rheological properties, and therefore display different morphologies. Our results show that novel non-spherical morphologies can be easily fabricated by tuning parameters such as diameter, concentration and collecting height, without the need for developing sophisticated on-chip platforms. Furthermore, we have monitored the temporal evolution of the droplets at the air-solution interface and proposed a possible mechanism for the deformation, supported by the experimental evidence.

These results can be applied for development of novel shape-tunable alginate microgels with specific surface properties. In addition, we showed that these non-spherical microgels can be used to construct complex superstructures assembled with spherical pNIPAAm microgels. These microgel superstructures can be potentially used as lock–key particles, self-propelled particles, and in modeling of macromolecules.

Conflict of interest

The authors declare no conflict of interest.

Acknowledgements

This work was supported by NSF Grant No. CBET-1150348. We thank Dr. Elaine Zhu and Raymond Seekell for assistance with the rheological measurements. We also thank Notre Dame Integrated Imaging Facility Center for the SEM measurement.

References

Asthana, A., Kim, K. O., Perumal, J., Kim, D. M., & Kim, D. P. (2009). Facile single step fabrication of microchannels with varying size. *Lab on a Chip*, *9*(8), 1138–1142.

Bajpai, S. K., & Sharma, S. (2004). Investigation of swelling/degradation behaviour of alginate beads crosslinked with Ca^{2+} and Ba^{2+} ions. *Reactive & Functional Polymers*, *59*(2), 129–140.

Bonino, C. A., Krebs, M. D., Saquing, C. D., Jeong, S. I., Shearer, K. L., Alsberg, E., et al. (2011). Electrospinning alginate-based nanofibers: From blends to crosslinked low molecular weight alginate-only systems. *Carbohydrate Polymers*, *85*(1), 111–119.

Capretto, L., Mazzitelli, S., Luca, G., & Nastruzzi, C. (2010). Preparation and characterization of polysaccharidic microbeads by a microfluidic technique: Application to the encapsulation of Sertoli cells. *Acta Biomaterialia*, *6*(2), 429–435.

Chan, E. S., Lee, B. B., Ravindra, P., & Poncelet, D. (2009). Prediction models for shape and size of ca-alginate macrobeads produced through extrusion-dripping method. *Journal of the Colloid and Interface Science*, *338*(1), 63–72.

Daimon, M., & Masumura, A. (2007). Measurement of the refractive index of distilled water from the near-infrared region to the ultraviolet region. *Applied Optics*, *46*(18), 3811–3820.

Dalmoro, A., Angela, B. A., Lamberti, G., Grassi, M., & Amore, M. (2012). Pharmaceutical applications of biocompatible polymer blends containing sodium alginate. *Advances in Polymer Technology*, *31*(3), 219–230.

Datta, S. S., Kim, S. H., Paulose, J., Abbaspourrad, A., Nelson, D. R., & Weitz, D. A. (2012). Delayed buckling and guided folding of inhomogeneous capsules. *Physical Review Letters*, *109*(13), 134302.

Dendukuri, D., Pregibon, D. C., Collins, J., Hatton, T. A., & Doyle, P. S. (2006). Continuous-flow lithography for high-throughput microparticle synthesis. *Nature Materials*, *5*(5), 365–369.

Du, Y., Lo, E., Ali, S., & Khademhosseini, A. (2008). Directed assembly of cell-laden microgels for fabrication of 3D tissue constructs. *Proceedings of the National Academy of Sciences of the United States of America*, *105*(28), 9222–9227.

Erb, R. M., Son, H. S., Samanta, B., Rotello, V. M., & Yellen, B. B. (2009). Magnetic assembly of colloidal superstructures with multipole symmetry. *Nature*, *457*(7232), 999–1002.

Esteban, Ó., Marvá, F., & Martínez-Antón, J. C. (2009). Optical constants of a sodium alginate polymer in the UV–vis range. *Optical Materials*, *31*(4), 696–699.

Fiddes, L. K., Young, E. W., Kumacheva, E., & Wheeler, A. R. (2007). Flow of microgel capsules through topographically patterned microchannels. *Lab on a Chip*, *7*(7), 863–867.

Gazori, T., Khoshayand, M. R., Azizi, E., Yazdizade, P., Nomani, A., & Haririan, I. (2009). Evaluation of alginate/chitosan nanoparticles as antisense delivery vector: Formulation, optimization and in vitro characterization. *Carbohydrate Polymers*, *77*(3), 599–606.

Hu, Y., Wang, J., Li, C., Wang, Q., Wang, H., Zhu, J., et al. (2013). Janus photonic crystal microspheres: Centrifugation-assisted generation and reversible optical property. *Langmuir*, *29*, 15529–15534.

Han, Y., Alsayed, A. M., Nobili, M., Zhang, J., Lubensky, T. C., & Yodh, A. G. (2006). Brownian motion of an ellipsoid. *Science*, *314*(5799), 626–630.

Hirama, H., Kambe, T., Aketagawa, K., Ota, T., Moriguchi, H., & Torii, T. (2013). Hyper alginate gel microbead formation by molecular diffusion at the hydrogel/droplet interface. *Langmuir*, *29*(2), 519–524.

Hong, L., Cacciuto, A., Luijten, E., & Granick, S. (2006). Clusters of charged Janus spheres. *Nano Letter*, *6*(11), 2510–2514.

Hu, Y., Wang, Q., Wang, J., Zhu, J., Wang, H., & Yang, Y. (2012). Shape controllable microgel particles prepared by microfluidic combining external ionic crosslinking. *Biomicrofluidics*, *6*(2), 26502–265029.

Ji, X. H., Cheng, W., Guo, F., Liu, W., Guo, S. S., He, Z. K., et al. (2011). On-demand preparation of quantum dot-encoded microparticles using a droplet microfluidic system. *Lab on a Chip*, *11*(15), 2561–2568.

Kanai, T., Lee, D., Shum, H., Shah, R. K., & Weitz, D. A. (2010). Gel-Immobilized colloidal crystal shell with enhanced thermal sensitivity at photonic wavelengths. *Advanced Materials*, *22*, 4998–5002.

Kang, D. H., Jung, H. S., Ahn, N., Yang, S. M., Seo, S., Suh, K. Y., et al. (2014). Janus-compartmental alginate microbeads having polydiacetylene liposomes and magnetic nanoparticles for visual Lead (II) detection. *ACS Applied Materials & Interfaces*, *6*, 10631–10637.

Lee, B. B., Ravindra, P., & Chan, E. S. (2013). Size and shape of calcium alginate beads produced by extrusion dripping. *Chemical Engineering & Technology*, *36*(10), 1627–1642.

Lee, K., Yoon, J., Rahmanic, S., Hwang, S., Bhaskar, S., Mitragotri, S., et al. (2012). Spontaneous shape reconfigurations in multicompartmental microcylinders. *Proceedings of the National Academy of Sciences*, *109*(40), 16057–16062.

Lee, K. Y., & Mooney, D. J. (2012). Alginate: Properties and biomedical applications. *Progress in Polymer Science*, *37*(1), 106–126.

Liakos, I., Rizzello, L., Bayer, I. S., Pompa, P. P., Cingolani, R., & Athanassiou, A. (2013). Controlled antiseptic release by alginate polymer films and beads. *Carbohydrate Polymers*, *92*(1), 176–183.

Lin, Y. S., Yang, C. H., Hsu, Y. Y., & Hsieh, C. L. (2013). Microfluidic synthesis of tail-shaped alginate microparticles using slow sedimentation. *Electrophoresis*, *34*(3), 425–431.

Liu, K., Ding, H., Liu, J., Chen, Y., & Zhao, X. (2006). Shape-controlled production of biodegradable calcium alginate gel microparticles using a novel microfluidic device. *Langmuir*, *22*, 9453–9457.

Liu, S., Deng, R., Li, W., & Zhu, J. (2012). Polymer microparticles with controllable surface textures generated through interfacial instabilities of emulsion droplets. *Advanced Functional Materials*, *22*, 1692–1697.

Loudet, J., Alsayed, A., Zhang, J., & Yodh, A. (2005). Capillary interactions between anisotropic colloidal particles. *Physical Review Letters*, *94*(1), 018301–018304.

Lu, Y., Yin, Y. D., & Xia, Y. N. (2001). Three-dimensional photonic crystals with non-spherical colloids as building blocks. *Advanced Materials*, *13*(6), 415–420.

Madivala, B., Vandebril, S., Fransaer, J., & Vermant, J. (2009). Exploiting particle shape in solid stabilized emulsions. *Soft Matter*, *5*(8), 1717–1727.

Maeda, K., Onoe, H., Takinoue, M., & Takeuchi, S. (2012). Controlled synthesis of 3D multi-compartmental particles with centrifuge-based microdroplet formation from a multi-barrelled capillary. *Advanced Materials*, *24*(10), 1340–1346.

Marquis, M., Davy, J., Fang, A., & Renard, D. (2014). Microfluidics-assisted diffusion self-assembly: Toward the control of the shape and size of pectin hydrogel microparticles. *Biomacromolecules*, *15*(5), 1568–1578.

Martinez, C. J., Kim, J. W., Ye, C., Ortiz, I., Rowat, A. C., Marquez, M., et al. (2012). A microfluidic approach to encapsulate living cells in uniform alginate hydrogel microparticles. *Macromolecular Bioscience*, *12*(7), 946–951.

Mele, E., Fragouli, D., Ruffilli, R., De Gregorio, G. L., Cingolani, R., & Athanassiou, A. (2013). Complex architectures formed by alginate drops floating on liquid surfaces. *Soft Matter*, *9*(27), 6338–6343.

Mondiot, F., Chandran, S. P., Mondain-Monval, O., & Loudet, J. C. (2009). Shape-induced dispersion of colloids in anisotropic fluids. *Physical Review Letters*, *103*(23), 238303–238304.

Muro, S., Garnacho, C., Champion, J. A., Leferovich, J., Gajewski, C., Schuchman, E. H., et al. (2008). Control of endothelial targeting and intracellular delivery of therapeutic enzymes by modulating the size and shape of ICAM-1-targeted carriers. *Molecular Therapy*, *16*(8), 1450–1458.

Nisisako, T., Torii, T., Takahashi, T., & Takizawa, Y. (2006). Synthesis of monodisperse bicolored Janus particles with electrical anisotropy using a microfluidic Co-Flow system. *Advance Materials*, *18*, 1152–1156.

Nie, Z., Seo, M., Xu, S., Lewis, P. C., Mok, M., Kumacheva, E., et al. (2008). Emulsification in a microfluidic flow-focusing device: Effect of the viscosities of the liquids. *Microfluidics and Nanofluidics*, *5*(5), 585–594.

Qiu, C., Chen, M., Yan, H., & Wu, H. K. (2007). Generation of uniformly sized alginate microparticles for cell encapsulation by using a soft-lithography approach. *Advanced Materials*, *19*(12), 1603–1607.

Shah, R. K., Shum, H. C., Rowat, A. C., Lee, D., Agresti, J. J., Utada, A. S., et al. (2008). Designer emulsions using microfluidics. *Materials Today*, *11*(4), 18–27.

Shang, L., Shangguan, F., Cheng, Y., Lu, J., Xie, Z., Zhao, Y., et al. (2013). Microfluidic generation of magnetoresponsive Janus photonic crystal particles. *Nanoscale*, *5*, 9553–9557.

Still, T., Chen, K., Alsayed, A. M., Aptowicz, K. B., & Yodh, A. G. (2013). Synthesis of micrometer-size poly(*N*-isopropylacrylamide) microgel particles with homogeneous crosslinker density and diameter control. *Journal of the Colloid and Interface Science*, *405*, 96–102.

Tan, W. H., & Takeuchi, S. (2007). Monodisperse alginate hydrogel microbeads for cell encapsulation. *Advanced Materials*, *19*(18), 2696–2701.

Tian, G., Park, S., Lee, M. J., Huck, B., McAllister, F., Hill, C. P., et al. (2011). An asymmetric interface between the regulatory and core particles of the proteasome. *Nature Structral Molecular Biology*, *18*(11), 1259–1267.

Wang, A., Cui, Y., Li, J., & van Hest, J. C. M. (2012). Fabrication of gelatin microgels by a "cast" strategy for controlled drug release. *Advanced Functional Materials*, *22*(13), 2673–2681.

Wang, L. X., & Bloomfield, V. A. (1990). Osmotic-pressure of semidilute solutions of flexible, globular, and stiff-chain polyelectrolytes with added salt. *Macromolecules*, *23*(1), 194–199.

Wang, Y., Wang, Y., Zheng, X., Yi, G. R., Sacanna, S., Pine, D. J., et al. (2014). Three-dimensional lock and key colloids. *Journal of the American Chemistry Society*, *136*(19), 6866–6869.

Xu, S., Nie, Z., Seo, M., Lewis, P., Kumacheva, E., Stone, H. A., et al. (2005). Generation of monodisperse particles by using microfluidics: Control over size, shape, and composition. *Angewandte Chemie International Edition*, *44*(5), 724–728.

Yan, J., Bloom, M., Bae, S. C., Luijten, E., & Granick, S. (2012). Linking synchronization to self-assembly using magnetic Janus colloids. *Nature*, *491*(7425), 578–581.

Yi, G. R., Pine, D. J., & Sacanna, S. (2013). Recent progress on patchy colloids and their self-assembly. *Journal of Physics: Condensed Matter*, *25*(19), 193101.

Yoo, J. W., & Mitragotri, S. (2010). Polymer particles that switch shape in response to a stimulus. *Proceedings of the National Academy of Sciences*, *107*(25), 11205–11210.

Zamanian, B., Masaeli, M., Nichol, J. W., Khabiry, M., Hancock, M. J., Bae, H., et al. (2010). Interface-directed self-assembly of cell-laden microgels. *Small*, *6*(8), 937–944.

Zhao, Y., Gu, H., Xie, Z., Shum, H., Wang, B., & Gu, Z. (2013). Bioinspired multifunctional Janus particles for droplet manipulation. *Journal of the American Chemical Society*, *135*, 54–57.